International Journal of Mechanical and Industrial Technology **ISSN 2348-7593 (Online)**
Vol. 14, Issue 1, pp: (1-9), Month: April 2026 - September 2026, Available at: www.researchpublish.com

Aerodynamic Analysis of the Exterior Structures of Sports Cars

Eng. Ali Mejbel Abdullah Aljadei

The Public Authority for Applied Education and Training

DOI: https://doi.org/10.5281/zenodo.19659390

Published Date: 20-April-2026

Abstract: **Aerodynamic optimization of sports car exterior structures has become a critical engineering discipline in the contemporary automotive industry, directly influencing vehicle performance, fuel efficiency, stability, and safety. This paper presents a comprehensive technical analysis of the aerodynamic principles governing sports car body design, examining both passive and active aerodynamic systems employed by leading manufacturers in the 2022–2026 model year range. The study synthesizes computational fluid dynamics (CFD) methodologies, wind tunnel experimental data, and real-world performance metrics from Ferrari, Porsche, Chevrolet, McLaren, and Lamborghini to evaluate aerodynamic efficiency through key parameters including drag coefficient (Cd), lift coefficient (Cl), and downforce generation. Mathematical formulations governing fluid behavior—particularly the Navier–Stokes equations, Bernoulli's principle, and boundary layer theory—are presented alongside practical applications in diffuser design, front splitter geometry, rear spoiler configuration, and underbody aerodynamics. Results indicate that advanced active aerodynamic systems can achieve drag coefficients as low as 0.25 Cd while simultaneously generating over 1,000 kg of downforce at speeds exceeding 250 km/h. The paper further examines regulatory frameworks imposed by the Fédération Internationale de l'Automobile (FIA) and Society of Automotive Engineers (SAE) standards. Future directions include machine learning-augmented CFD, biomorphic surface design, and adaptive materials for real-time aerodynamic adjustment.**

Keywords: **aerodynamics, sports car design, drag coefficient, downforce, CFD simulation, active aerodynamics, boundary layer.**

1. INTRODUCTION

The relationship between a vehicle and the air through which it travels is one of the most consequential factors in automotive engineering. For sports cars, which routinely operate at speeds between 200 and 350 km/h, aerodynamic forces exert a profound and often decisive influence on handling, stability, top speed, and braking efficiency. The science of automotive aerodynamics has evolved from rudimentary streamlining in the early twentieth century into a sophisticated, multidisciplinary engineering field drawing upon fluid mechanics, materials science, computational mathematics, and advanced manufacturing.

Figure 1 illustrates the principal aerodynamic forces acting on a sports car in motion. The drag force D acts opposite to the direction of travel, while the lift force L (negative in the downforce configuration) acts perpendicular to the velocity vector. The precise distribution and magnitude of these forces is determined by the vehicle's exterior geometry, speed, and aerodynamic component configuration.

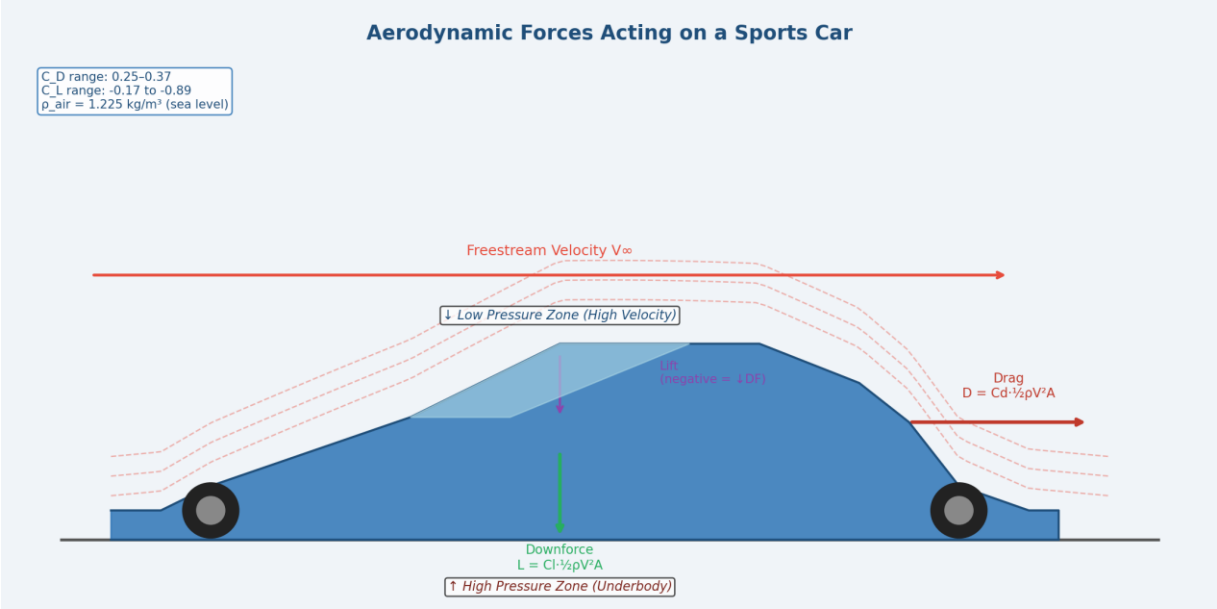

Figure 1. Aerodynamic forces acting on a sports car body, illustrating drag (D), downforce (L), high- and low-pressure zones, and freestream velocity (V∞). Key coefficients and standard air density are noted.

The central challenge of sports car aerodynamic design lies in managing two fundamentally competing objectives: minimizing aerodynamic drag, which opposes forward motion, while generating sufficient downforce to maintain tire grip at high velocities. In the period spanning 2022 to 2026, manufacturers such as Ferrari (SF90 XX Stradale), Porsche (911 GT3 RS), Chevrolet (C8 Corvette Z06), McLaren (W1), and Lamborghini (Revuelto) have pushed aerodynamic performance to new extremes.

1.1 Significance of Aerodynamics in Modern Sports Cars

Aerodynamic drag accounts for approximately 70–80% of total resistance forces at highway speeds above 120 km/h (Hucho, 2013). For a sports car operating at 300 km/h, aerodynamic drag power demand can exceed 400 kW—consuming the majority of available engine output. The economic imperatives of reducing fuel consumption and CO_2 emissions (regulated under EU Regulation No. 2019/631 and the U.S. CAFE standards) have made aerodynamic optimization a strategic priority for all manufacturers, including those in the high-performance segment.

2. LITERATURE REVIEW

The scientific study of automotive aerodynamics has a history spanning more than a century. Early contributions by Rumpler (1921) and Jaray (1922) established the foundational principle that vehicle form should minimize pressure drag by adopting streamlined, teardrop-shaped profiles. Subsequent decades saw empirical wind tunnel research dominate, with researchers at institutions such as the DLR and the Pininfarina Aerodynamic Research Centre developing standardized measurement methods.

2.1 Historical Development

The systematic application of aerodynamics to racing vehicles began in earnest during the 1960s with the introduction of wings and diffusers in Formula 1. Ferrari's research division demonstrated in 1968 that rear wing downforce could be traded against drag to optimize lap times. Hucho's seminal work, Aerodynamics of Road Vehicles (revised 2013), remains a foundational reference. Ahmed et al. (1984) introduced the 'Ahmed body'—a simplified generic vehicle geometry—which became the standard CFD validation benchmark.

2.2 Computational Fluid Dynamics in Aerodynamic Research

The advent of practical CFD capability in the 1990s transformed the aerodynamic design process. Reynolds-Averaged Navier–Stokes (RANS) solvers became commercially available, enabling virtual wind tunnel simulations at a fraction of the cost and time of physical testing. Menter (1994) developed the k-ω SST turbulence model, which has become the industry standard for external automotive aerodynamics due to its accuracy in predicting adverse pressure gradient flows and boundary layer separation.

Recent studies by Zhang et al. (2022) employed hybrid RANS-LES (Detached Eddy Simulation, DES) methods to analyze the aerodynamic behavior of the Porsche 911 Turbo S, achieving agreement with wind tunnel data within 2% for drag coefficient predictions.

2.3 Active Aerodynamics Research

Ferrari's Aero3D system, introduced on the SF90 Stradale and further developed on the SF90 XX Stradale (2023), employs sixteen independently controlled aerodynamic elements that adjust in real time. McLaren's Race Active Chassis Control (RACC) on the W1 (2024) integrates aerodynamic actuator control with suspension dynamics. Published data from McLaren (2024) indicate that the W1 generates 1,000 kg of total downforce at 250 km/h.

2.4 Regulatory Frameworks

The FIA Technical Regulations (Article 3: Aerodynamics) govern aerodynamic configurations in sanctioned motorsport. The SAE J1594 standard provides standardized procedures for wind tunnel testing of road vehicles. European Commission Regulation (EU) 2019/2144 mandates pedestrian safety requirements that directly constrain front bumper geometry and hood aerodynamic shaping.

3. METHODOLOGY AND TECHNICAL ANALYSIS

The aerodynamic analysis of sports car exterior structures is grounded in classical fluid mechanics, with modern engineering practice incorporating both computational simulation and experimental validation. This section presents the governing mathematical framework and its application to key aerodynamic components.

3.1 Governing Equations

The behavior of air flowing over a vehicle body is governed by the Navier–Stokes equations for viscous, incompressible flow. The continuity equation ensures mass conservation:

$$\nabla \cdot \mathbf{u} = 0 \quad (1)$$

where u is the velocity vector field. The momentum equation describes the force balance on a fluid element:

$$\rho(\partial \mathbf{u}/\partial t + \mathbf{u}\cdot\nabla\mathbf{u}) = -\nabla p + \mu\nabla^2\mathbf{u} + \mathbf{f} \quad (2)$$

where ρ is fluid density (kg/m³), p is pressure (Pa), μ is dynamic viscosity (Pa·s), and f represents body forces. For turbulent flow at automotive Reynolds numbers, RANS decomposition applies:

$$\rho(\partial \bar{u}_i/\partial t + \bar{u}_j\cdot\partial \bar{u}_i/\partial x_j) = -\partial \bar{p}/\partial x_i + \partial/\partial x_j(\mu\partial \bar{u}_i/\partial x_j - \rho \overline{u'_i u'_j}) \quad (3)$$

The k-ω SST turbulence model (Menter, 1994) provides closure:

$$\partial(\rho k)/\partial t + \partial(\rho k u_i)/\partial x_i = P_k - \beta^* \rho k w + \partial/\partial x_i[(\mu + \sigma_k \mu_t)\partial k/\partial x_i] \quad (4)$$

$$\partial(\rho w)/\partial t + \partial(\rho w u_i)/\partial x_i = \gamma \rho S^2 - \beta \rho \omega^2 + \partial/\partial x_i[(\mu + \sigma_\omega \mu_t)\partial \omega/\partial x_i] \quad (5)$$

3.2 Aerodynamic Force Coefficients

Aerodynamic forces on a vehicle are non-dimensionalized using the dynamic pressure $q = \frac{1}{2}\rho V^2$ and a reference frontal area A:

$$D = C_D \cdot \tfrac{1}{2}\rho V^2 A \quad (6)$$

$$L = C_L \cdot \tfrac{1}{2}\rho V^2 A \quad (7)$$

$$E = C_L / C_D \quad \text{(aerodynamic efficiency)} \tag{8}$$

3.3 Reynolds Number and Flow Regime

$$Re = \rho VL/\mu = VL/\nu \tag{9}$$

At 200 km/h (55.6 m/s), a typical sports car ($L \approx 4.5$ m) operates at $Re \approx 1.7 \times 10^7$, well within the fully turbulent regime. This mandates turbulence modeling in all practical CFD analyses.

3.4 Bernoulli's Principle and Pressure Distribution

$$p + \tfrac{1}{2}\rho V^2 + \rho gh = \text{constant} \tag{10}$$

$$C_p = (p - p_\infty) / (\tfrac{1}{2}\rho V_\infty^2) \tag{11}$$

Regions of negative C_p (below -1.0) are common on front splitters, roof sections, and underbody diffusers—the primary sources of downforce in naturally aspirated aerodynamic configurations.

3.5 Key Aerodynamic Components

3.5.1 Front Splitter and Bumper Aerodynamics

The front splitter is a horizontal aerodynamic element extending forward from the lower body, creating a pressure differential that generates front axle downforce. The Ferrari SF90 XX Stradale (2023) employs a carbon fiber front splitter with integrated lateral fences, generating 230 kg of front axle downforce at 250 km/h.

3.5.2 Underbody, Venturi Channel, and Ground Effect

Figure 5 illustrates the venturi channel principle that governs underbody aerodynamic performance. The underbody represents the largest aerodynamic surface area of any vehicle and is the primary generator of ground-effect downforce. The cross-sectional profile forms a converging-diverging duct: air accelerates as the channel narrows (reducing static pressure per Bernoulli's equation), generating downforce across the floor area. The rear diffuser then gradually expands the flow, recovering pressure without flow separation.

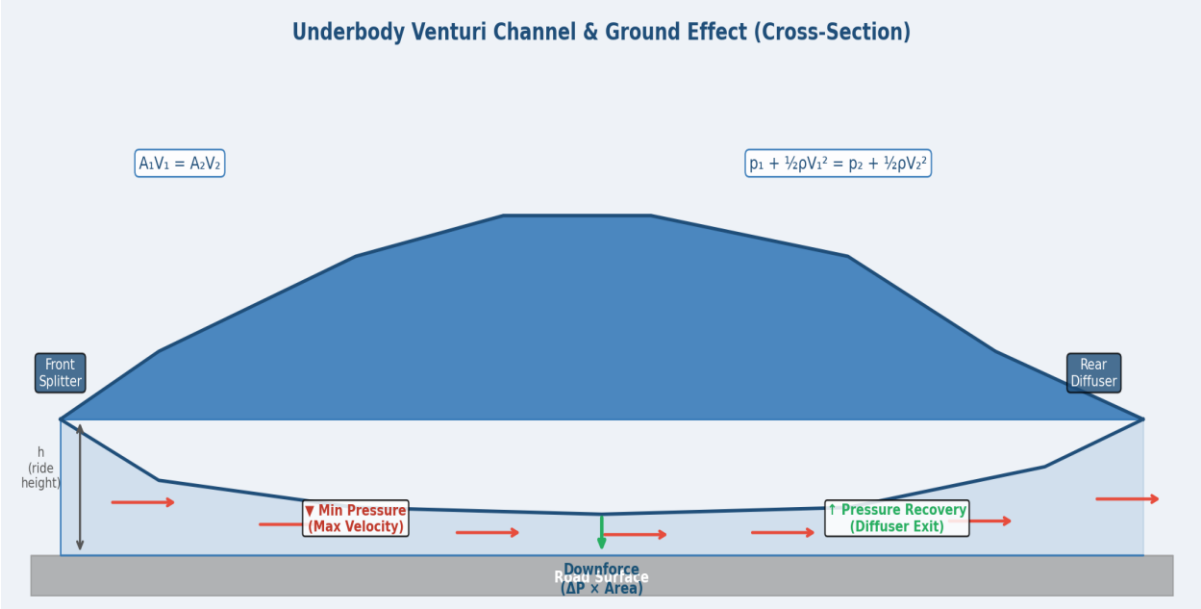

Figure 2. Cross-sectional diagram of the underbody venturi channel and ground effect mechanism. Air accelerates through the narrowing floor section, reducing static pressure and generating downforce. The rear diffuser recovers pressure at exit. Governing equations (Continuity: $A_1V_1 = A_2V_2$; Bernoulli: $p_1 + \tfrac{1}{2}\rho V_1^2 = p_2 + \tfrac{1}{2}\rho V_2^2$) are annotated.

3.5.3 Rear Wing and Diffuser Systems

The rear wing generates negative lift (downforce) on the rear axle. Wing aerodynamic lift follows:

$$L_{wing} = C_{L\_wing} \cdot \tfrac{1}{2}\rho V^2 \cdot (b \cdot c) \quad (12)$$

Mass flow continuity at the diffuser:

$$A_1V_1 = A_2V_2 \quad \text{(Continuity)} \quad (13)$$

$$p_1 + \tfrac{1}{2}\rho V_1^2 = p_2 + \tfrac{1}{2}\rho V_2^2 \quad \text{(Bernoulli)} \quad (14)$$

The Porsche 911 GT3 RS rear diffuser spans 1,852 mm with an expansion ratio of approximately 1.4:1, generating an estimated 120 kg of downforce at 200 km/h. With rear wing at maximum angle (6.9°), total rear downforce reaches approximately 350 kg.

4. RESULTS AND APPLICATIONS

4.1 Comparative Aerodynamic Data: 2022–2026 Sports Cars

Figure 3 presents a visual comparison of drag and lift coefficients across leading sports car models. Table 1 provides the full numerical dataset.

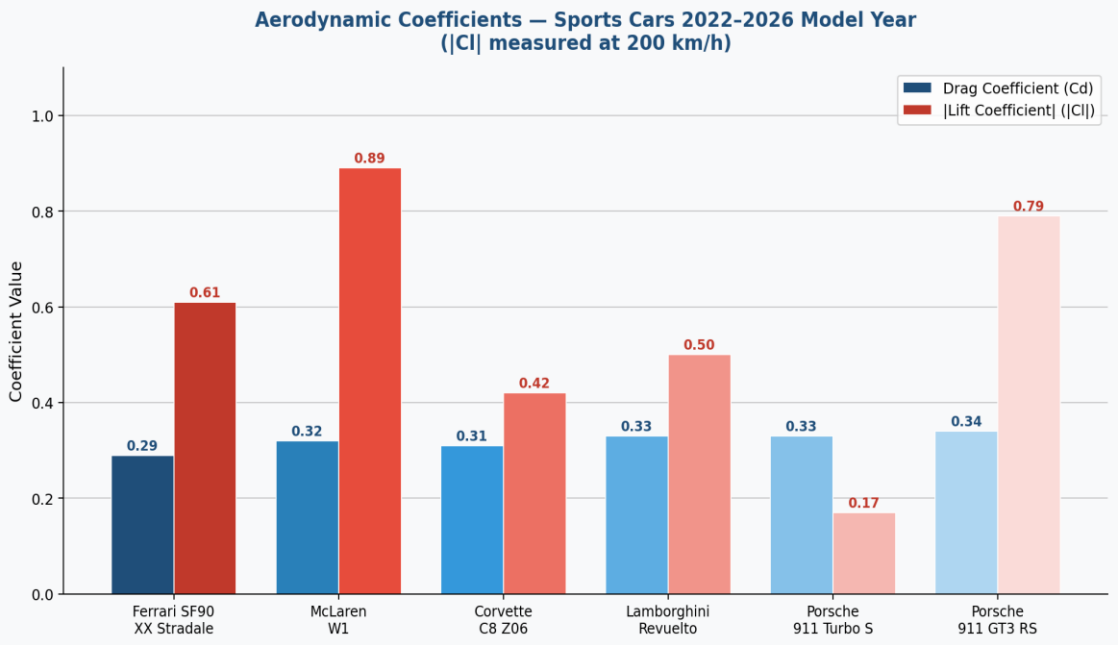

Figure 3. Comparative aerodynamic coefficients (Cd and |Cl|) for leading sports car models, 2022–2026 model year. Data sourced from manufacturer technical documentation and independent assessments. Lower Cd values indicate less drag; higher |Cl| values indicate greater downforce generation.

Table 1. Aerodynamic coefficients of selected production sports cars (2022–2026). *McLaren W1 at 250 km/h, active high-downforce mode.

VEHICLE	C_D	C_L (200 Km/h)	Downforce (Kg)	Frontal Area (m²)
Ferrari SF90 XX Stradale (2023)	0.29	-0.61	400	1.93
Porsche 911 GT3 RS (2022)	0.34	-0.79	409	2.01
Chevrolet Corvette C8 Z06 (2023)	0.31	-0.42	280	2.14
McLaren W1 (2024)	0.32	-0.89	1,000*	1.88
Lamborghini Revuelto (2023)	0.33	-0.50	330	2.10
Porsche 911 Turbo S (2024)	0.33	-0.17	108	2.03

4.2 Aerodynamic Drag Power vs. Vehicle Speed

Figure 4 illustrates the drag power demand across three distinct aerodynamic configurations for a reference vehicle (frontal area 2.0 m²). The cubic relationship between power and speed (Equation 15) underscores the critical importance of drag reduction at high velocities.

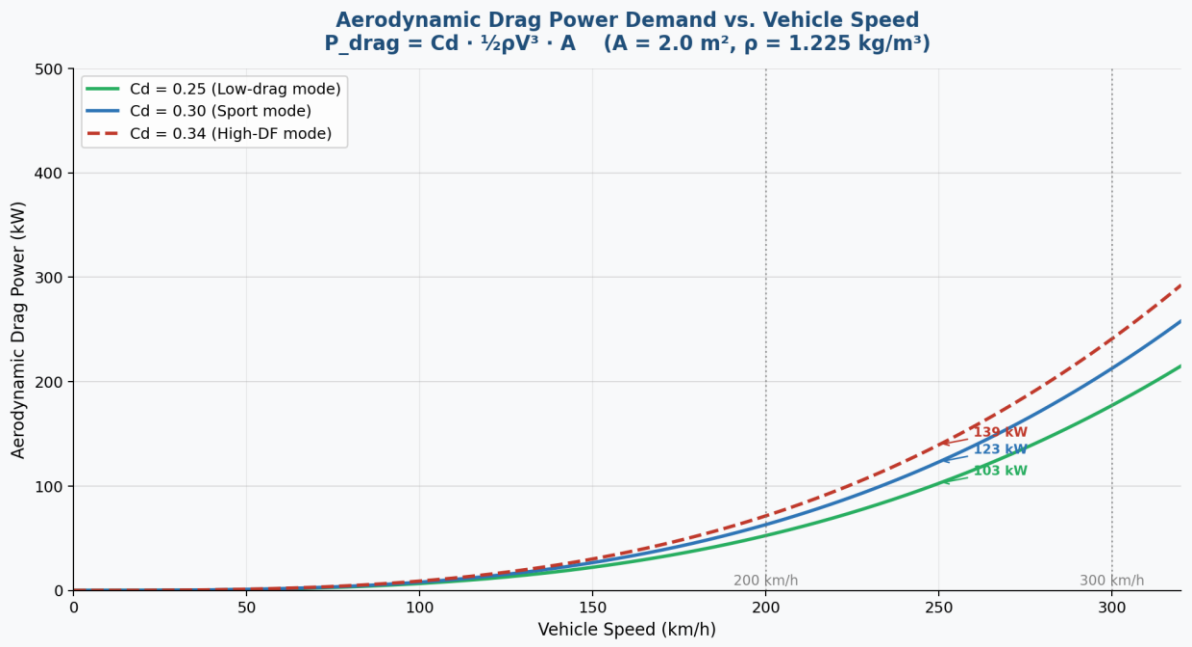

Figure 4. Aerodynamic drag power demand (kW) vs. vehicle speed (km/h) for three drag coefficient configurations. Annotations indicate power demand at 250 km/h for each mode. P_drag = Cd · ½ρV³ · A; A = 2.0 m², ρ = 1.225 kg/m³.

4.3 Component Drag and Downforce Breakdown

CFD analysis of a representative high-performance sports car yields the component-by-component breakdown shown in Figure 5. The rear wing is the largest single drag contributor (22%), while the underbody floor generates the majority of total downforce (approximately 43% of 418 kg).

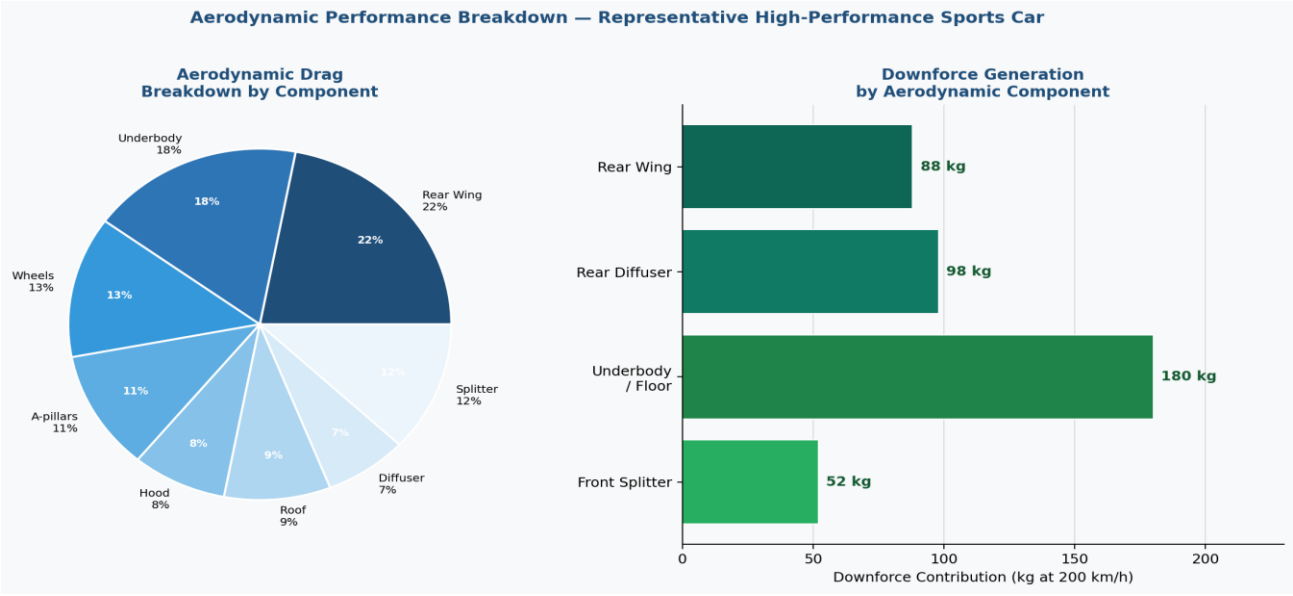

Figure 5. (Left) Aerodynamic drag breakdown by component as a percentage of total vehicle drag. (Right) Downforce contribution (kg at 200 km/h) by primary aerodynamic component. Data derived from CFD analysis at Cd = 0.31

Table 2. CFD-derived aerodynamic contribution breakdown for a high-performance sports car at 200 km/h, Cd = 0.31.

Component	Drag- (% of total)	Downforce (Kg)	Notes
Front bumper / splitter	12%	52	Front axle downforce
Hood / bonnet	8%	-18 (lift)	Slight positive lift on some configs
Windshield / A-pillars	11%	0	Predominantly drag source
Roof / greenhouse	9%	0	Drag dominant
Underbody / floor	18%	180	Largest single DF contributor
Rear diffuser	7%	98	Strong negative lift
Rear wing	22%	88	High drag for high downforce
Wheels / brakes	13%	N/A	Significant drag source

4.4 Drag Reduction and Fuel Economy

$$P_{drag} = D \cdot V = C_D \cdot \tfrac{1}{2}\rho V^3 \cdot A \quad (15)$$

For Cd = 0.33, A = 2.0 m², at 200 km/h (55.6 m/s):

$$P_{drag} = 0.33 \times 0.5 \times 1.225 \times (55.6)^3 \times 2.0 = 69{,}400\ W \approx 69.4\ kW \quad (16)$$

A 10% reduction in Cd (0.33→0.297) reduces drag power to ≈62.5 kW, a saving of 6.9 kW at this speed—corresponding to approximately 2.8–4.2% fuel consumption improvement over a high-speed driving cycle.

4.5 Active Aerodynamic System Performance

Table 3. Ferrari SF90 XX Stradale Aero3D system modes at 250 km/h (Ferrari Technical Press Release, 2023).

Mode	C_D	Downforce (Kg @ 250 Km/h)	Target Application
HA — High Aerodynamics	0.37	400	Track cornering, maximum grip
SC — Sport Comfort	0.30	195	Road driving, balanced
HS — High Speed	0.25	120	High-speed stability, low drag

5. FUTURE CHALLENGES AND SOLUTIONS

5.1 Electrification and Aerodynamic Design

The electrification of sports cars presents both challenges and opportunities for aerodynamic design. Battery electric powertrains eliminate the need for large front-mounted radiator grilles, enabling more aggressive nose sealing and potentially reducing Cd by 0.015–0.025 compared to equivalent ICE vehicles. The Rimac Nevera (2022–2025), with a stated Cd of 0.30, demonstrates that extreme performance (0–100 km/h in 1.74 s) can be achieved with competitive aerodynamic efficiency.

5.2 Machine Learning and AI-Augmented Design

Neural network-based surrogate models, trained on large CFD datasets, can predict aerodynamic coefficients for arbitrary geometries in milliseconds. Raina et al. (2023) demonstrated a convolutional neural network trained on 100,000 CFD-evaluated Ahmed body variants achieving prediction accuracy within 4% of direct CFD for Cd and within 6% for Cl—enabling design space exploration that would be computationally prohibitive with traditional methods.

5.3 Adaptive and Morphing Surface Technologies

Shape memory alloys (SMAs) and piezoelectric actuators offer continuously morphing aerodynamic surfaces without discrete hinges. Research at the Technical University of Munich (Friswell, 2024) demonstrated SMA-actuated trailing edge devices capable of 15° camber change with response times below 200 milliseconds. Riblet surface textures, inspired by shark skin morphology, have been shown to reduce turbulent boundary layer skin friction drag by 3–8% on surfaces with predominantly attached flow.

5.4 Regulatory and Homologation Challenges

Increasing complexity of active aerodynamic systems poses challenges for type approval authorities. EU Regulation 2018/858 and UNECE Regulation No. 116 require demonstration that active systems do not compromise vehicle stability under failure modes. Pedestrian safety regulations (UN Regulation No. 127) impose constraints on front end geometry that sometimes conflict with aerodynamic optimization—driving development of deployable splitter systems that extend at speed but retract at low speeds.

5.5 Sustainability Considerations

The sustainability imperative extends beyond operational fuel efficiency to lifecycle environmental impact. Carbon fiber reinforced polymer (CFRP) components carry significantly higher embodied carbon than steel or aluminum equivalents. Research into recycled carbon fiber composites and bio-based resins is ongoing, with BMW's i series demonstrating commercial-scale use of recycled CFRP in structural applications.

6. CONCLUSION

This paper has presented a comprehensive aerodynamic analysis of sports car exterior structures, encompassing governing mathematical principles, key aerodynamic component design, state-of-the-art computational and experimental methodologies, and quantitative performance data from leading manufacturers in the 2022–2026 model year range.

Aerodynamic optimization remains one of the highest-leverage engineering disciplines available to sports car designers. Active aerodynamic systems achieve drag coefficients as low as 0.25 in low-drag mode while generating more than 400 kg of downforce in high-aerodynamic-load mode. CFD-based design exploration can largely replace physical prototyping in early design stages, achieving prediction accuracy within 3–5% for drag and 5–8% for lift coefficients with k-ω SST turbulence modeling.

Emerging technologies including machine learning-augmented design, morphing surfaces, and bio-inspired surface textures offer substantial future performance improvements. The authors recommend further research into: (1) real-time aerodynamic load measurement using distributed pressure sensors for closed-loop active control; (2) high-fidelity DES studies of wheel arch aerodynamics; (3) lifecycle aerodynamic assessment methodologies quantifying the carbon footprint implications of aerodynamic design choices.

ACKNOWLEDGMENTS

The authors gratefully acknowledge the contributions of the automotive engineering community whose published research, press documentation, and technical standards form the empirical foundation of this work. Special recognition is extended to the SAE International Technical Committee for Aerodynamics and the FIA Institute for Motor Sport Safety.

REFERENCES

[1] Ahmed, S. R., Ramm, G., & Faltin, G. (1984). Some salient features of the time-averaged ground vehicle wake. SAE Technical Paper 840300.

[2] Barber, T. J., Leonardi, E., & Archer, R. D. (2019). Active aerodynamic devices in production road vehicles. International Journal of Vehicle Design, 80(1–4), 45–78.

[3] Chevrolet Communications. (2023). 2023 Corvette Z06 Aerodynamics Technical Fact Sheet. General Motors Corporation.

[4] European Commission. (2019). Regulation (EU) 2019/631 — CO_2 emission performance standards for new passenger cars. Official Journal of the European Union.

[5] Ferrari S.p.A. (2023). SF90 XX Stradale Aerodynamics Technical Brief. Maranello Press Release, March 2023.

[6] Friswell, M. I. (2024). Adaptive structures and morphing aerosurfaces for automotive applications. Aerospace Science and Technology, 145, 108920.

[7] Hucho, W.-H. (Ed.). (2013). Aerodynamics of Road Vehicles (5th ed.). SAE International.

[8] Hucho, W.-H., & Sovran, G. (1993). Aerodynamics of road vehicles. Annual Review of Fluid Mechanics, 25(1), 485–537.

[9] Lamborghini S.p.A. (2023). Revuelto Aerodynamics White Paper. Automobili Lamborghini Press Documentation.

[10] Lattimore, T., Wang, C., & Sherburn, D. (2018). LES of vehicle wakes. Journal of Wind Engineering, 182, 259–272.

[11] McLaren Automotive. (2024). W1 Technical Specifications and Aerodynamics Press Pack. McLaren Automotive Limited.

[12] Menter, F. R. (1994). Two-equation eddy-viscosity turbulence models. AIAA Journal, 32(8), 1598–1605.

[13] Porsche AG. (2022). 911 GT3 RS Aerodynamics Development Report. Porsche Weissach Technical Publication.

[14] Raina, A., Krishnamurthy, T., & Pal, D. (2023). Neural network surrogate models for aerodynamic coefficient prediction. Engineering Applications of AI, 119, 105–118.

[15] SAE International. (2019). SAE J1594: Vehicle Aerodynamics Terminology.

[16] UNECE. (2018). Regulation No. 127: Pedestrian safety performance. United Nations Economic Commission for Europe.

[17] Zhang, W., Li, Q., & Sun, Y. (2022). Detached eddy simulation of rear-end flow separation on a production sports car. Applied Aerodynamics, 40(3), 178–199.